Chemical Science

EDGE ARTICLE

View Article Online
View Journal | View Issue

Cite this: *Chem. Sci.*, 2018, **9**, 4083

Energetic insights into two electron transfer pathways in light-driven energy-converting enzymes†

Keisuke Kawashima[a] and Hiroshi Ishikita *[ab]

Received 26th January 2018
Accepted 28th March 2018

DOI: 10.1039/c8sc00424b

rsc.li/chemical-science

We report redox potentials (E_m) for one-electron reduction for all chlorophylls in the two electron-transfer branches of water-oxidizing enzyme photosystem II (PSII), photosystem I (PSI), and purple bacterial photosynthetic reaction centers (PbRC). In PSI, E_m values for the accessory chlorophylls were similar in both electron-transfer branches. In PbRC, the corresponding E_m value was 170 mV less negative in the active L-branch (B_L) than in the inactive M-branch (B_M), favoring $B_L^{\bullet-}$ formation. This contrasted with the corresponding chlorophylls, Chl_{D1} and Chl_{D2}, in PSII, where $E_m(Chl_{D1})$ was 120 mV more negative than $E_m(Chl_{D2})$, implying that to rationalize electron transfer in the D1-branch, Chl_{D1} would need to serve as the primary electron donor. Residues that contributed to $E_m(Chl_{D1}) < E_m(Chl_{D2})$ simultaneously played a key role in (i) releasing protons from the substrate water molecules and (ii) contributing to the larger cationic population on the chlorophyll closest to the Mn_4CaO_5 cluster (P_{D1}), favoring electron transfer from water molecules. These features seem to be the nature of PSII, which needs to possess the proton-exit pathway to use a protonated electron source—water molecules.

The crystal structures of photosystem II (PSII), photosystem I (PSI) and purple bacterial photosynthetic reaction centers from *Rhodobacter sphaeroides* (PbRC) show a pseudo-twofold axis of symmetry, forming the following heterodimeric protein subunit pairs: D1/D2 in PSII, PsaA/PsaB in PSI, and L/M in PbRC.[1–6] In PbRC, electron-transfer branches (L- and M-branches) proceed from a pair of bacteriochlorophyll *a* (BChl*a*) (P_L and P_M) *via* accessory BChl*a* (B_L and B_M), bacteriopheophytin *a* (BPheo*a*) (H_L and H_M), and ubiquinone (Q_A and Q_B). In PSII, the corresponding cofactors are the pair of chlorophyll *a* (Chl*a*) (P_{D1} and P_{D2}), accessory Chl*a* (Chl_{D1} and Chl_{D2}), pheophytin *a* (Pheo*a*) ($Pheo_{D1}$ and $Pheo_{D2}$), and plastoquinone (Q_A and Q_B) of D1- and D2-branches, and in PSI, the pair of Chl*a* and the 13^2 epimer[7] (P_A and P_B), accessory Chl*a* (A_{-1A} and A_{-1B}), acceptor Chl*a* (A_{0A} and A_{0B}), and phylloquinone (A_{1A} and A_{1B}) of A- and B-branches (Fig. 1). In PSI (*i.e.*, a type-I reaction center), electron transfer occurs in both A- and B-branches,[8] whereas in PbRC and PSII (*i.e.*, type-II reaction centers) electron transfer predominantly occurs along L- and D1-branches, respectively. In PbRC and PSII, excitation of BChl*a* and Chl*a* leads to charge separation on the L- and D1-branches and formation of the cationic $[P_L/P_M]^{\bullet+}$ and $[P_{D1}/P_{D2}]^{\bullet+}$ states, respectively (*e.g.*,[9]). Regardless of the structural similarities between the two reaction centers,[1] many features are different.[9] The $[P_L/P_M]^{\bullet+}$ state has a redox potential (E_m) of 500 mV for one-electron oxidation[10] and accepts an electron from an outer protein subunit, cytochrome c_2 (or tetraheme cytochrome in PbRC from *Blastochloris viridis*). The $[P_{D1}/P_{D2}]^{\bullet+}$ state has a high E_m (>1100 mV)[11–13] and ultimately abstracts electrons from the substrate water molecules at the catalytic Mn_4CaO_5 moiety in D1 *via* redox-active D1-Tyr161 (TyrZ). Redox-active D2-Tyr160 (TyrD) exists at the symmetrical position in D2. Basic D2-Arg180 and D2-His61 near TyrD on the D2 side contribute to the larger $P_{D1}^{\bullet+}$ population than $P_{D2}^{\bullet+}$ in $[P_{D1}/P_{D2}]^{\bullet+}$,[13] *i.e.*, electrostatically pushing the cation onto P_{D1},[14] thereby favoring electron transfer from the substrate water molecules in D1.[15] Unlike PbRC, which only requires an electron transfer pathway, PSII also requires a proton transfer pathway from the substrate water molecules because the water molecules are protonated electron sources. In PSII, the release of protons (H^+) has been observed in response to changes in the oxidation state (S_n) of the oxygen-evolving complex, and it occurs with a typical stoichiometry of 1 : 0 : 1 : 2 for the $S_0 \rightarrow S_1 \rightarrow S_2 \rightarrow S_3 \rightarrow S_0$ transitions, respectively.[16] Proton transfer may proceed *via* different pathways depending on the S-state transitions.[17–19] The nature of the proton-conducting O4-water chain,[20] which is composed exclusively of water molecules, is consistent with and may explain the pH-independence of proton transfer in the S_0 to S_1 transition.[16] On the other hand, the pH-dependent rate constant for the S_2-to-S_3 transition[16]

[a]*Department of Applied Chemistry, The University of Tokyo, 7-3-1 Hongo, Bunkyo-ku, Tokyo 113-8654, Japan. E-mail: hiro@appchem.t.u-tokyo.ac.jp*

[b]*Research Center for Advanced Science and Technology, The University of Tokyo, 4-6-1 Komaba, Meguro-ku, Tokyo 153-8904, Japan. Fax: +81-3-5452-5083; Tel: +81-3-5452-5056*

† Electronic supplementary information (ESI) available. See DOI: 10.1039/c8sc00424b

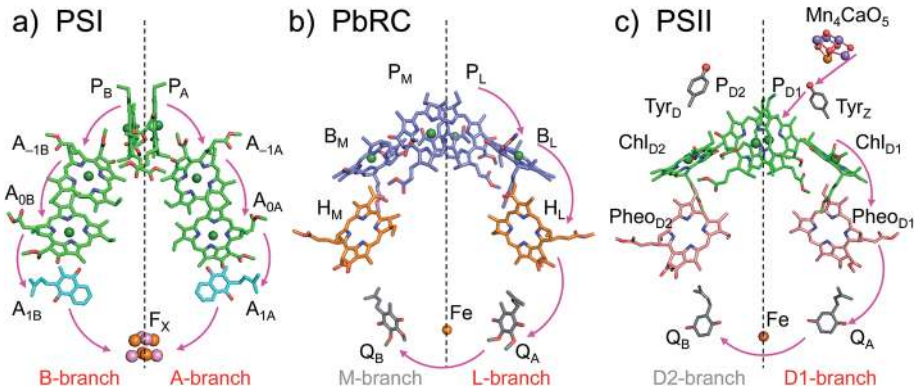

Fig. 1 Electron transfer chains in photosynthetic reaction centers of (a) PSI (PDB code 1JB0), (b) PbRC (PDB code 3I4D), and (c) PSII (PDB code 3ARC). Pink arrows indicate electron transfer. Dotted lines indicate pseudo-C_2 axes. Electron-transfer active branches are red labeled, whereas inactive branches are gray labeled.

indicates the involvement of ionizable groups in the proton transfer pathway (*e.g.*, the pathway *via* D1-Asp61 [21,22]). Acquirement of the Mn_4CaO_5 cluster seems to induce a polar protein environment near the electron acceptor $[P_{D1}/P_{D2}]^{\bullet+}$ and may alter the energetics of electron transfer along the D1-branch with respect to that along the L-branch in PbRC.

The free energy difference between cofactors (*e.g.*, electronically excited $[P_L/P_M]^*$ and $[P_L/P_M]^{\bullet+}H_L^{\bullet-}$) was discussed experimentally (*e.g.*,[23]) and theoretically (*e.g.*,[24]). However, detailed E_m values of the cofactors for one-electron reduction in active L- and D1-branches as well as inactive M- and D2-branches have not yet been experimentally determined and are a matter of debate (*e.g.*,[25]). Although we reported calculated E_m values for one-electron oxidation in PSI, PbRC, and PSII,[13,26] these E_m values are more associated with distributions of the cationic states over the (B)Chl*a* pairs (*e.g.*, $[P_A/P_B]^{\bullet+}$ (ref. 27) and $[P_{D1}/P_{D2}]^{\bullet+}$ (ref. 13)). Due to a lack of E_m values of the cofactors for one-electron reduction in PbRC, PSI, and PSII, it remains still unclear why electron transfer occurs in both A- and B-branches in PSI, whereas in PbRC and PSII electron transfer predominantly occurs along L- and D1-branches.

Here, we present E_m values of Chl*a*, Pheo*a*, BChl*a*, and BPheo*a* for one-electron reduction in both electron-transfer branches of PbRC, PSI, and PSII; the E_m values were calculated using the crystal structures, solving the linear Poisson–Boltzmann equation, and considering the protonation states of all titratable sites in the entire proteins.

Results

E_m for accessory chlorophylls

In PSI, $E_m(A_{-1A})$ and $E_m(A_{-1B})$ as well as $E_m(A_{0A})$ and $E_m(A_{0B})$ are at essentially the same level in the cyanobacterial[2] (Fig. 2a) and plant[6] (Fig. S1†) PSI crystal structures. $E_m(A_{0A}) = -1042$ mV and $E_m(A_{0B}) = -1023$ mV (Fig. 2a), obtained using the cyanobacterial[2] PSI crystal structure, are consistent with the experimentally estimated values, *e.g.*, $E_m(A_0) = -1050$ mV [28] and -1040 mV.[29]

In PbRC, $E_m(B_L)$ is ~170 mV less negative than $E_m(B_M)$ based on the crystal structure analyzed at 2.01 Å resolution (Protein Data Bank (PDB) code 3I4D) (Fig. 2b). $E_m(B_L)$ and $E_m(B_M)$ were also calculated based on other PbRC crystal structures (*e.g.*, PDB codes, 1M3X[3] and 1EYS;[30] Fig. S2†) and show the same tendency.

In sharp contrast to PbRC, $E_m(Chl_{D1})$ is 120 mV more negative than $E_m(Chl_{D2})$ in the 1.9 Å PSII crystal structure[5] (Fig. 2c). At the Chl_{D1} and Chl_{D2} binding sites, "the PSII protein dielectric volume" (*i.e.*, "uncharged protein volume", which is ultimately comprised of van der Waals radii of all protein atoms) decreases the solvation of the Chl*a* cofactors, destabilizes Chl*a*$^{\bullet-}$, and thus lowers the $E_m(Chl_{D1})$ and $E_m(Chl_{D2})$ values. On the other hand, "the atomic charges of proteins" (*i.e.*, "protein charges") also affect E_m(Chl*a*); *e.g.*, negatively charged groups destabilize Chl*a*$^{\bullet-}$ and lower the $E_m(Chl_{D1})$ and $E_m(Chl_{D2})$ values. To identify the factors that differentiate between $E_m(Chl_{D1})$ and $E_m(Chl_{D2})$ in PSII, we analyzed contributions of "protein atomic charges" and "loss of solvation" to $E_m(Chl_{D1})$ and $E_m(Chl_{D2})$. Contributions of the protein atomic charges are predominantly responsible for the difference in the E_m values for accessory chlorophylls between PbRC and PSII, whereas contributions to E_m from the protein volume, which prevents the solvation of reduced accessory chlorophylls and thus lowers E_m, are much smaller (Table 1).

$E_m(Pheo_{D1})$ is -507 mV (Fig. 2c), which is consistent with the value of -499 mV [31] obtained using the 3.0 Å PSII crystal structure (PDB code 2AXT)[32] and the spectroelectrochemically determined value of -505 mV.[33]

$B_L^{\bullet-}$ stabilization in PbRC

In PbRC, electronic excitation of BChl*a* leads to the formation of the $(P_L/P_M)^{\bullet+}B_L^{\bullet-}$ state.[34] Fig. 2 shows that $E_m(B_L)$ is 170 mV less negative than $E_m(B_M)$, facilitating electron transfer along the L-branch. The asymmetry of the electron-transfer energetics is caused by the different contributions of charges on the residues and cofactors, not the different shapes of the proteins (*e.g.*, solvent accessibility near each BChl*a*) (Table 1). In particular, loop *a*–*b* and helix *cd* in the periplasm region and helix *d* in the transmembrane region, which are structurally conserved in PSII (Fig. 3), helped to stabilize $B_L^{\bullet-}$ with respect to $B_M^{\bullet-}$ (Table 2). Among the L/M-residue pairs, Phe-L181/Tyr-M210 in helix

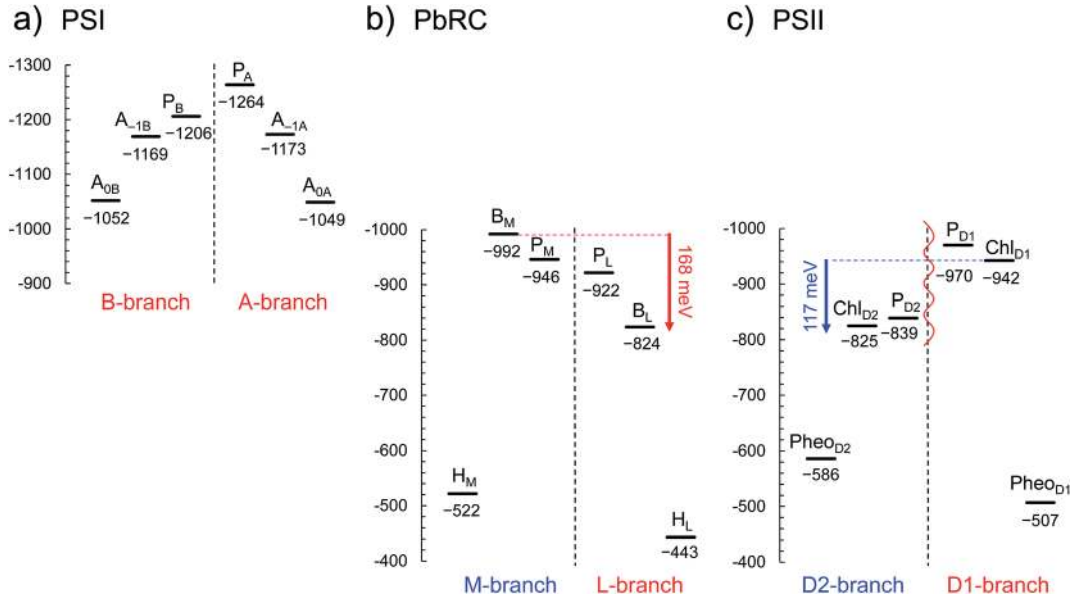

Fig. 2 E_m for one-electron reduction in the electron transfer chains in photosynthetic reaction centers of (a) PSI (PDB code 1JB0), (b) PbRC (PDB code 3I4D), and (c) PSII (PDB code 3ARC) in mV. Red and blue arrows indicate the E_m difference between accessory (B)Chl*a* cofactors in PbRC and PSII, respectively. The red wavy line indicates the weak electronic coupling (*i.e.*, uncoupling) between P_{D1} and P_{D2}.[49,50] Dotted lines indicate pseudo-C_2 axes. Electron-transfer active branches are red labeled, whereas inactive branches are blue labeled. See ref. 13 and 26 for calculated E_m values for one-electron oxidation in PSI, PbRC, and PSII.

Table 1 Contributions of the protein atomic charges and loss of solvation (*i.e.*, due to protein volume, which prevents the solvation of reduced chlorophylls and thus lowers E_m) to E_m for accessory chlorophylls in mV. The E_m differences between the two electron-transfer branches are listed in the brackets

Protein	PSI			PbRC			PSII		
Accessory chlorophyll	A_{-1B}	A_{-1A}		P_M	P_L		Chl_{D2}	Chl_{D1}	
E_m	−1169	−1173	(−4)	−992	−824	(168)	−825	−942	(−117)
In uncharged protein[a]	−1085	−1071	(14)	−851	−813	(38)	−1047	−1058	(−11)
In water	−798	−798	(0)	−641	−641	(0)	−798	−798	(0)
E_m shift (water to protein)	−371	−375	(−4)	−351	−183	(168)	−27	−144	(−117)
Due to protein charge	−84	−102	(−18)	−141	−11	(130)	222	116	(−106)
Due to loss of solvation	−287	−273	(14)	−210	−172	(38)	−249	−260	(−11)

[a] Calculated in the absence of all atomic partial charges of the proteins.

d ($E_m(B_L) - E_m(B_M) = 26$ mV), Tyr-L67/Glu-M95 in loop *a*–*b* (20 mV), and Asp-L155/Asp-M184 in helix *cd* (22 mV) provide the greatest contribution to $E_m(B_L) > E_m(B_M)$ (Table 3).

(i) *Asp-M184 and Glu-M95 at the binding interface of cytochrome c_2, decreasing $E_m(B_M)$.* Table 3 shows that Glu-M95 and Asp-M184 contribute to decreasing $E_m(B_M)$ (22 mV and 37 mV, respectively) and thus stabilizing $B_L^{\bullet-}$ with respect to $B_M^{\bullet-}$. From the observation of the PbRC–cytochrome c_2 co-crystal structure, Axelrod *et al.* concluded that Glu-M95 and Asp-M184 provide the largest electrostatic interaction with cytochrome c_2 (Fig. S3†).[35] Notably, among the 17 PbRC mutants, mutation of Asp-M184 to Lys exhibits the largest change, with a decrease in the binding constant with cytochrome c_2 by a factor of 800.[36] Thus, negatively charged Asp-M184 likely contributes not only to binding of the one-electron donor of PbRC (*i.e.*, cytochrome c_2) but also to electron transfer along the L-branch.

(ii) *How Tyr-M210 facilitates L-branch electron transfer.* Among all L/M-residue pairs in PbRC, the difference in the Phe-L181/Tyr-M210 pair in helix *d* contributes to the E_m difference the most, *i.e.*, increasing $E_m(B_L)$ with respect to $E_m(B_M)$, as suggested in theoretical analysis by Parson *et al.*[37] (Table 3). Indeed, mutations of Tyr-M210 to phenylalanine decreased the initial electron transfer with a time constant from 3.5 ps to 16 ps.[38] The PbRC crystal structure analyzed at 2.01 Å (PDB code 3I4D) shows that the polar –OH group of Tyr-M210 is oriented toward B_L, thus stabilizing $B_L^{\bullet-}$ and increasing $E_m(B_L)$. The –OH group cannot be oriented toward the methyl-keto (acetyl) group of P_M because the methyl site, rather than the keto site, is near the –OH group of Tyr-M210 (Fig. 4a).

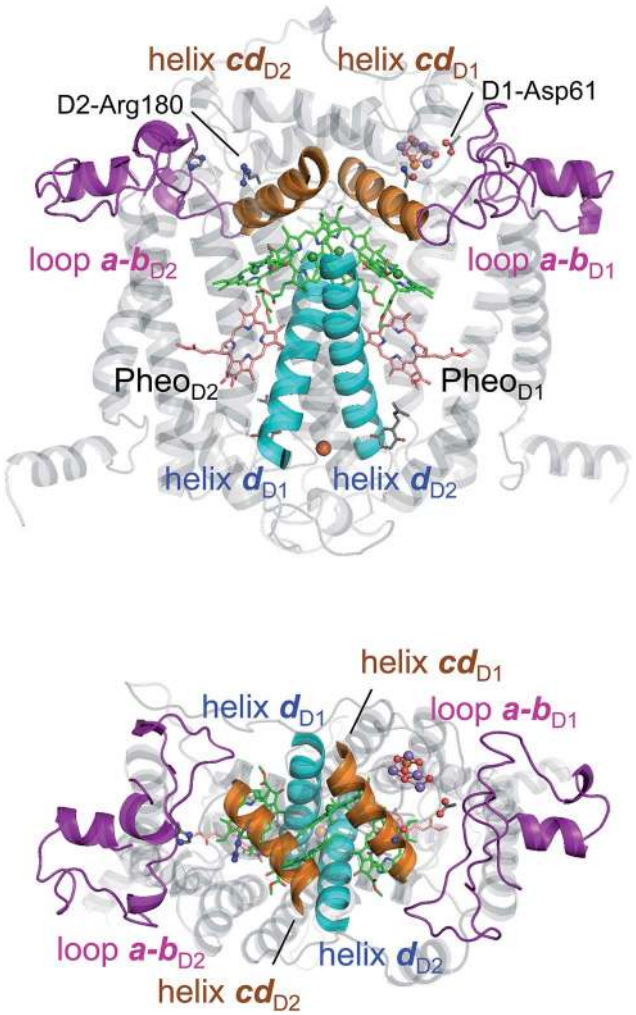

Fig. 3 Structural components of type-II reaction centers (*e.g.*, PSII).

In contrast to the 2.01 Å structure, the assignment of the methyl C and keto O atoms of P_M is opposite in the PbRC crystal structure analyzed at 1.87 Å (PDB code 2J8C);[4] the methyl-keto orientation allows the –OH group of Tyr-M210 to form an H-bond with the keto O atom of P_M (O_{PM}–$O_{TyrM210}$ = 3.4 Å; Fig. 4b). Thus, the methyl-keto orientation of P_M in the 1.87 Å structure cannot stabilize $B_L^{\bullet-}$ (Fig. S4†). However, the electron density map of all BChl*a* and Pheo*a* in the 1.87 Å structure,[4] except for P_L, indicates that the density is too low for the keto O atoms (red mesh in Fig. 4c), but too high for the methyl C atoms (green mesh in Fig. 4c) in the original assignment. Remarkably, the swapped assignment of the methyl-keto O and C atoms in P_M, B_L, B_M, H_L, and H_M in the 1.87 Å structure (refined 1.87 Å structure), which is consistent with the original assignment in the 2.01 Å structure, is in better agreement with the density with a decrease in an *R*-factor by 0.01% (Fig. 4d). Just by rotating the methyl-keto groups (forming the refined 1.87 Å structure), the E_m difference, *i.e.*, $E_m(P_L) - E_m(B_L)$, can be altered from −8 mV to −72 mV (Fig. S4†).

Hence, the methyl-keto orientations assigned in the 2.01 Å structure (PDB code 3I4D) appear to be relevant to the PbRC conformation; the –OH group of Tyr-M210 is predominantly oriented toward B_L, stabilizing $B_L^{\bullet-}$ and increasing $E_m(B_L)$.

Table 2 Contributions of the protein components to E_m for accessory chlorophylls in PbRC and PSII in mV. —, not applicable

Region	Component	$E_m(B_L) - E_m(B_M)$ in PbRC	$E_m(Chl_{D1}) - E_m(Chl_{D2})$ in PSII	Difference
Periplasm/lumen	Mn_4CaO_5[a]	—	56	—
	$2Cl^-$	—	−66	—
	Loop *a*–*b*	47	−86	−133
	Helix *cd*	40	−91	−131
	Others	−7	55	48
Transmembrane	Helix *a*	−7	7	14
	Helix *b*	−3	15	18
	Helix *c*	15	−50	−65
	Helix *d*	50	17	−33
	Helix *e*	−5	26	31
	Cofactors	17	−6	−23
Cytoplasm/stroma	Subunit H	−2	—	—
	Others	9	9	0

[a] Including ligand groups.

Table 3 Contributions of residues in subunits L and M to $E_m(B_L)$ and $E_m(B_M)$ in mV

	$E_m(B_L)$	$E_m(B_M)$		$E_m(B_L)$	$E_m(B_M)$	$E_m(B_L) - E_m(B_M)$
Phe-L181	0	22	Tyr-M210	44	−4	26
Val-L157	19	0	Thr-M186	−1	−4	22
Tyr-L67	0	0	Glu-M95	−2	−22	20
Ser-L178	−1	−21	Ala-M207	−7	−2	16
Asp-L155	−21	−5	Asp-M184	−6	−37	15

(iii) *Low dielectric volume near B_M provided by spheroidene and the Q_B side chain*. Around the Glu-M95/Asp-M184 moiety, approximately 30 hydrophobic residues from subunit M are in van der Waals contact with the carotenoid spheroidene (Fig. S5†).[39] The electrostatic influence of the negative charges at the Glu-M95/Asp-M184 moiety is likely to be less screened at B_M with respect to B_L, thus destabilizing $B_M^{\bullet-}$. For the same reason, the cluster of hydrophobic residues seems also to enhance the polar –OH group of Tyr-M210 to stabilize $B_L^{\bullet-}$. Hence, spheroidene, the cluster of hydrophobic residues, and the Q_B isoprene side chain (see below) may be the origin of the low effective dielectric constant reported near B_M with respect to B_L in the Stark effect spectrum[40] or the significantly small electric field along the M-branch suggested in electrostatic calculations.[24] It should be noted that there are no water channels identified near Chl_{D1} and Chl_{D2} in the PSII crystal structures.[41,42]

(iv) *The Q_B isoprene side chain, decreasing specifically $E_m(B_M)$*. The isoprene side chain of Q_B is oriented toward B_M and is partly in van der Waals contact with spheroidene, whereas that of Q_A is oriented away from B_L (Fig. S5†).

The isoprene side chain of Q_B in the PbRC crystal structure analyzed at 2.01 Å (PDB code 3I4D) is comprised of 56 C atoms. When the side chain of Q_B is shortened to 16 C atoms, as identified in the 1.87 Å PbRC crystal structure (PDB code 2J8C),[4] and the corresponding inner space is filled by water

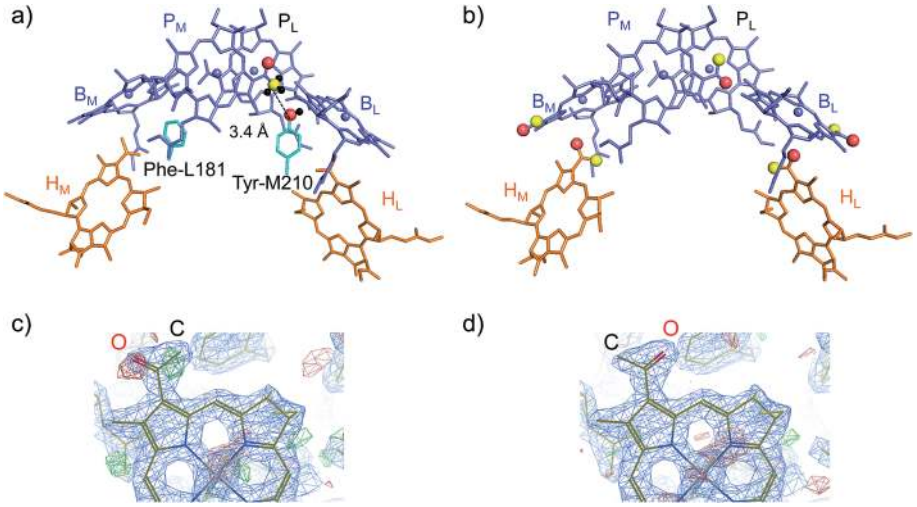

Fig. 4 (a) Orientations of the methyl-keto group in P_M (yellow ball for methyl C and red ball for keto O) and the hydroxyl group in Tyr-M210 (red ball for hydroxyl O) in the 2.01 Å-PbRC structure (PDB code 3I4D). (b) The methyl-keto groups in BChl*a* and BPheo*a* (yellow balls for methyl C and red balls for keto O) in the 1.87 Å-PbRC structure (PDB code 2J8C),[4] whose assignments of the keto O atom and the methyl C atom are opposite to those in the 2.01 Å-PbRC structure (PDB code 3I4D). (c) The original assignment of the methyl-keto group of B_L in the 1.87 Å-PbRC structure. The density is too low when the keto O atom is assumed (red mesh), whereas too much when the methyl C atom is assumed (green mesh). (d) The swapped assignment of the methyl-keto group of B_L in the 1.87 Å-PbRC structure.

(represented implicitly with the dielectric constant $\varepsilon_w = 80$), changes in E_m are predominantly observed at $E_m(B_M)$ with an increase of 57 mV (Fig. S6b†); this suggests that the isoprene chain of Q_B also contributes to the hydrophobic protein environment specifically for B_M, enhancing electrostatic interactions and destabilizing $B_M^{\bullet-}$.

Factors that are responsible for $E_m(Chl_{D1}) < E_m(Chl_{D2})$ in PSII

Table 2 shows that loop *a–b* (86 mV) and helix *cd* (91 mV) in the lumen region (Fig. 3) are responsible for $E_m(Chl_{D1}) < E_m(Chl_{D2})$ in PSII. Below we describe the key components that contribute to $E_m(Chl_{D1}) < E_m(Chl_{D2})$.

(i) *D1-Asp61/D2-His61 pair in loop a–b.* In the stromal/lumen region, loop *a–b* (that connects helices *a* and *b*) and helix *cd* (Fig. 3) seem most likely to characterize PSII with respect to PbRC (Table 2). Loop *a–b* is comprised of 55 residues in D1 (D1: 55–109) and 54 residues in D2 (D2: 55–108), which are almost twice as long as that in PbRC (26 residues in subunit L (L: 57–82) and 34 residues in subunit M (M: 79–112)). The region D2-Val55–Ser66 in PSII is structurally absent in PbRC (Fig. S7†). The insertion in PSII involves key residues for water oxidation, *e.g.*, D1-Ile60 (O_2-exiting pathway[43]), D1-Asp61 (proton transfer pathway[22,44]), D1-Glu65 (proton transfer pathway[22,45] and water channel[42]), and D2-His61 (proton transfer pathway for TyrD[44,46,47]). In particular, the D1-Asp61/D2-His61 pair decreases $E_m(Chl_{D1})$ by 98 mV (Table 4). The corresponding residues and proton transfer pathways are absent in PbRC.

(ii) *D2-Arg180 in helix cd, specifically increasing $E_m(Chl_{D2})$.* In PSII, lumenal helix *cd* (D1: 176–190/D2: 176–188 for PSII, Fig. 3) decreases $E_m(Chl_{D1})$ with respect to $E_m(Chl_{D2})$ by 131 mV, whereas in PbRC, lumenal helix *cd* (and L: 152–162/M: 179–192 for PbRC) increases $E_m(B_L)$ with respect to $E_m(B_M)$ by 40 mV (Table 2).

In particular, the D1-Asn181/D2-Arg180 pair in helix *cd* decreases $E_m(Chl_{D1})$ by 73 mV with respect to $E_m(Chl_{D2})$ (Table 4). D1-Asn181 also serves as the Cl-1 binding site[5] in the proton-conducting E65/E312 water channel.[42] D2-Arg180 is located at the entrance of the proton transfer pathway for TyrD[44,46] and provides the driving force.[47] Furthermore, the D1-Asn181/A2-Arg180 pair is responsible for a larger $P_{D1}^{\bullet+}$ population than $P_{D2}^{\bullet+}$ (ref. 13), which facilitates electron transfer from substrate water molecules at the Mn_4CaO_5 moiety in D1.

(iii) *Influence of Mn_4CaO_5.* E_m values calculated using the Mn-depleted PSII crystal structure[48] are similar to those obtained using the 1.9 Å PSII crystal structure (Fig. S8†). Calculated protonation states in the Mn-depleted PSII crystal structure show that the ligand residues (D1-Asp170, D1-Glu189, D1-His332, D1-Glu333, the carboxy-terminal D1-Ala344, and CP43-Glu354) and the H-bond partner (D1-His337) are fully protonated, which could compensate for loss of the cationic Mn_4CaO_5 cluster (Table S1†). Hence, the inorganic Mn_4CaO_5 component itself is not a main factor that determines E_m and the energetics of electron transfer.[13,26]

Discussion

Different mechanism of single-branch electron transfer between PbRC and PSII

$E_m(B_L)$ is 170 mV less negative than $E_m(B_M)$ in PbRC. In contrast, the corresponding $E_m(Chl_{D1})$ value is 120 mV more negative than $E_m(Chl_{D2})$ in PSII. These controversial E_m profiles imply that the mechanisms of single-branch electron transfer are different between PbRC and PSII even though both are type-II reaction centers. The initial electron transfer from the P_L/P_M pair to B_L is 100 meV downhill in the L-branch and 50 meV uphill in the M-branch (Fig. 2). This energy difference should

Table 4 Contributions of residues in D1 and D2 to $E_m(Chl_{D1})$ and $E_m(Chl_{D2})$ in mV. —, not applicable

	$E_m(Chl_{D1})$	$E_m(Chl_{D2})$		$E_m(Chl_{D1})$	$E_m(Chl_{D2})$	$E_m(Chl_{D1}) - E_m(Chl_{D2})$
D1-Asp61	−72	−26	D2-His61	23	75	−98
D1-Asn181[a]	5	−1	D2-Arg180	44	123	−73
Cl-1[a]	−91	−38	—	—	—	−53
D1-Asp170	−75	−30	D2-Phe169	−2	−6	−42
D1-Tyr161 +D1-His190[b]	−8	12	D2-Tyr160 +D2-His189[b]	5	24	−39
D1-Glu65 +D1-Asn315[c]	−11	−2	D2-Ser65 +D2-Glu312[c]	−36	−15	−30
D1-Glu189	−47	−26	D2-Phe188	2	5	−24
D1-Ser305	1	3	D2-Glu302	−43	−22	−23
D1-Asp59	−32	−11	D2-Tyr59	0	2	−23
D1-Asn301	2	0	D2-Asp297	−50	−29	−20

[a] Cl-1 and D1-Asn181 interact directly ($Cl^- \cdots N_{D1\text{-}Asn181} = 3.31$ Å[5]). [b] D1-Tyr161 and D1-His190 form an H-bond, sharing a proton. D2-Tyr160 and D2-His189 form an H-bond, sharing a proton. [c] D1-Glu65 and D2-Glu312 form an H-bond, sharing a proton.

facilitate L-branch electron transfer. If P_{D1} and P_{D2} could form the strongly coupled P_{D1}/P_{D2} special pair and function as an initial electron donor, electronic excitation of the P_{D1}/P_{D2} pair might possibly have led to electron transfer in the D2-branch, since $E_m(Pheo_{D2})$ is sufficiently higher than $E_m(Chl_{D2})$ (Fig. 2). However, the electronic coupling between P_{D1} and P_{D2} (85 to 150 cm^{-1} (ref. 49 and 50)) in PSII is much weaker than that between P_L and P_M (500 to 1000 cm^{-1} (ref. 51)) in PbRC. In addition, the longest wavelength pigment is thought to be Chl_{D1} in PSII.[50,52] Given that Chl_{D1} is the primary electron donor (*i.e.*, Chl*a*, where excitation occurs due to the lowest site-energy) in PSII (*e.g.*,[53]), the calculated E_m values indicate that electron transfer can occur in the D1-branch because of the sufficiently high $E_m(Pheo_{D1})$ value (−500 mV [31,33] and Fig. 2).

Hence, it seems likely that PSII activates electron transfer in the D1-branch (i) by uncoupling the P_{D1}/P_{D2} pair (*i.e.*, making both electron-transfer branches electronically completely isolated) and (ii) by employing Chl_{D1} as the primary electron donor; in contrast, PbRC activates electron transfer in the L-branch by increasing $E_m(B_L)$ with respect to $E_m(B_M)$ in the presence of the strongly coupled P_L/P_M pair.

Influence of the periplasm/lumen region on E_m for accessory (B)Chl*a*

In PbRC, among the total E_m difference of 168 mV between B_L and B_M (where $E_m(B_L) > E_m(B_M)$), 80 mV originates from the periplasm region, namely loop *a*–*b* (47 mV) and helix *cd* (40 mV); in PSII, among the total E_m difference of −117 mV between Chl_{D1} and Chl_{D2} (where $E_m(Chl_{D1}) < E_m(Chl_{D2})$), −132 mV originates from the corresponding lumen region, namely loop *a*–*b* (−86 mV) and helix *cd* (−91 mV) (Table 2). Thus, loop *a*–*b* and helix *cd* in the periplasm/lumen region primarily contribute to the different E_m profiles (Fig. 2) for PbRC and PSII.

In PbRC, acidic residues Asp-M184 in helix *cd* and Glu-M95 in loop *a*–*b*, which contribute to $E_m(B_L) > E_m(B_M)$ (Table 3), serve as an H-bond network for the binding of cytochrome c_2, the source of electrons for $[P_L/P_M]^{\bullet+}$. In PSII, basic residues D2-Arg180 in helix *cd* and D2-His61 in loop *a*–*b*, which contribute to $E_m(Chl_{D1}) < E_m(Chl_{D2})$ (Table 4), serve as a proton-conducting H-bond

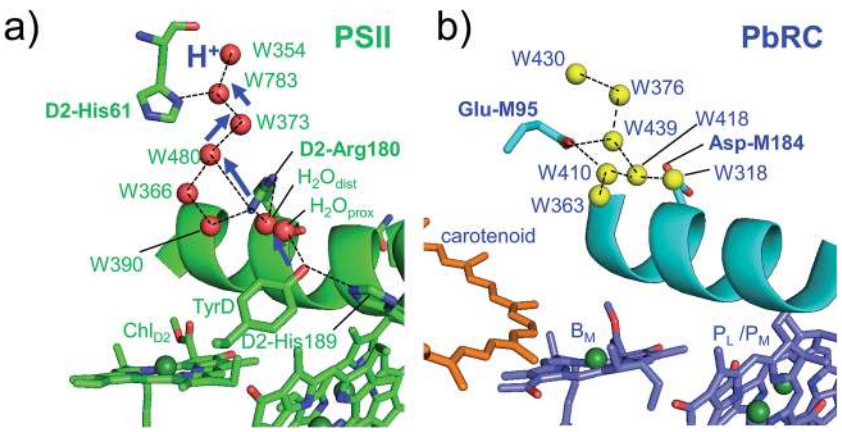

Fig. 5 (a) H-bond network of water molecules (red balls) near Chl_{D2} in PSII (green), serving as a proton transfer pathway from TyrD (blue arrows)[44,47] and (b) the corresponding H-bond network of water molecules (yellow balls) near B_M in PbRC (cyan). The carotenoid molecule (spheroidene) exists only in PbRC.

network proceeding from TyrD[44,46,47] and also increase the $P_{D1}^{\bullet+}$ population with respect to $P_{D2}^{\bullet+}$ in $[P_{D1}/P_{D2}]^{\bullet+}$.[13]

Intriguingly, Asp-M184 in helix *cd* and Glu-M95 in loop *a*–*b* in PbRC correspond to D2-Arg180 in helix *cd* and D2-His61 in loop *a*–*b* in PSII, respectively (Fig. 5 and S8†). Furthermore, even water molecules in the proton transfer pathway from TyrD in PSII seem to be structurally conserved on the binding surface near Asp-M184 and Glu-M95 in PbRC (Fig. 5b). These structural features imply that the cytochrome c_2 binding network in PbRC and the proton transfer pathway from TyrD in PSII have a common origin, which differentiate the mechanism of single-branch electron transfer between PbRC and PSII.

From the involvement of Asp-M184 in the binding interface with cytochrome c_2 and correspondence of Asp-M184 to D2-Arg180 (Fig. S9†), the electrostatic differences in the periplasm/lumen regions are likely associated with the difference in sources of electrons–cytochrome c_2/H_2O.

Type-I reaction centers with respect to type-II reaction centers

In PSII, residues that increase the E_m difference between Chl_{D1} and Chl_{D2} (Table 2) are mostly identical to those that have been identified to increase the E_m difference between P_{D1} and P_{D2} significantly[13] (*e.g.*, D1-Asp61/D2-His61, D1-Asn181/D2-Arg180, D1-Asp170/D2-Phe169, and D1-Glu189/D2-Phe188). These results suggest that the same PSII protein electrostatic environment (discussed above) is responsible for asymmetry in energetics of the electron transfer branches (Fig. 2) as well as the cationic state distribution over the $[P_{D1}/P_{D2}]^{\bullet+}$.[13]

In PSI, the protein electrostatic environments of PsaA and PsaB are quite similar and no residues have been identified to induce the E_m difference between P_A and P_B significantly.[27] Indeed, $E_m(A_{-1A})$ and $E_m(A_{-1B})$ are also similar (Fig. 2a and S1†) and there are no residues that induce the E_m difference between A_{-1A} and A_{-1B}. It seems likely that the similar protein electrostatic environment of PsaA and PsaB is a main factor that plays a role in keeping both branches open for electron transfer in PSI.

Concluding remarks

In PSII, substrate water molecules need to release protons when acting as an electron donor; thus, both electron and proton transfer pathways are expected to proceed from the substrate water molecules. The proton transfer pathway from O4 and the electron transfer pathway toward $P_{D1}^{\bullet+}$ go along the same axis in the opposite directions (Fig. 6), which allows PSII to use the common protein electrostatic environment for both transfer of electrons (e^-) and protons (H^+) without competing. It seems plausible that $E_m(Chl_{D1}) < E_m(Chl_{D2})$ in PSII, which is obviously inconsistent with $E_m(B_L) > E_m(B_M)$ in PbRC, is due to a compromise between release of protons and release of electrons from the substrate water molecules using the common protein electrostatic environment and could have been overcome (i) by uncoupling the P_{D1}/P_{D2} pair and (ii) by employing Chl_{D1} as the primary electron donor.

Hence, it is likely not a coincidence that the D1/D2 residue pairs, which are responsible for $E_m(Chl_{D1}) < E_m(Chl_{D2})$ (*e.g.*, D1-Asn181/D2-Arg180 and D1-Asp61/D2-His61), can also serve as (i) electrostatically pushing the cation onto P_{D1} [basic residues in D2],[14] providing a larger $P_{D1}^{\bullet+}$ population than $P_{D2}^{\bullet+}$ (ref. 13) and thereby facilitating electron transfer from substrate water molecules in D1.[15] The presence of low pK_a groups (*i.e.*, acidic residues) near the proton releasing Mn_4CaO_5 site [acidic residues in

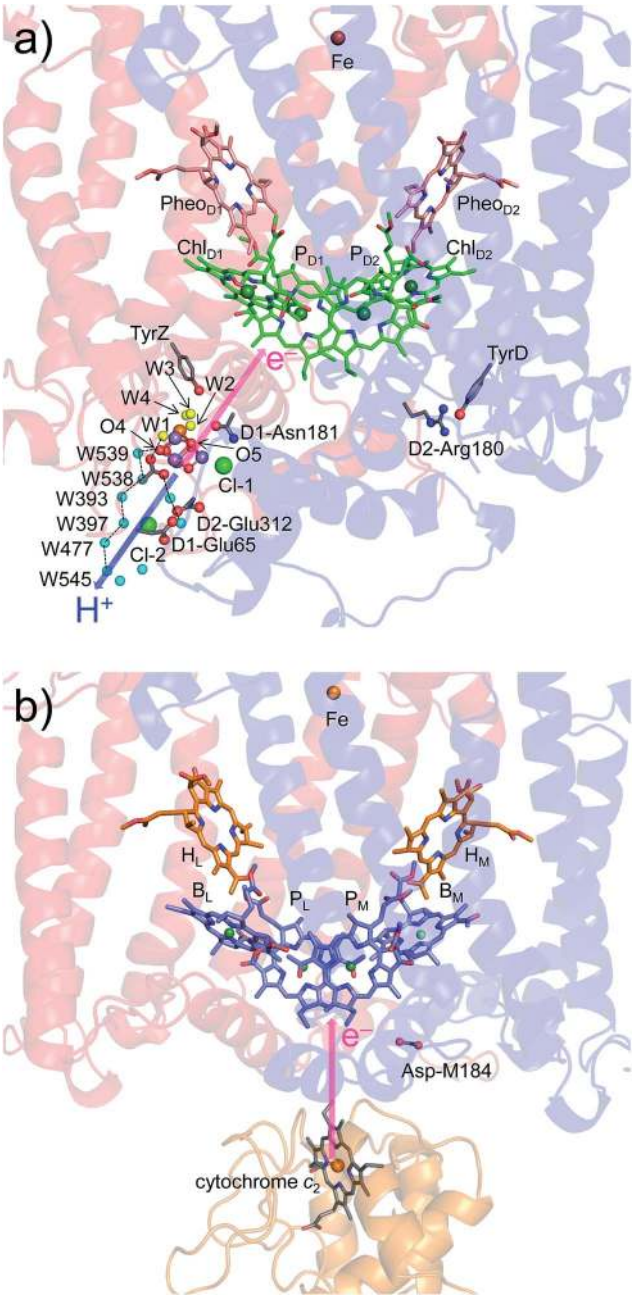

Fig. 6 Locations of the electron transfer (pink arrows) and proton transfer (blue arrow) pathways in (a) PSII and (b) PbRC. Ligand water molecules are indicated by yellow balls and other water molecules by cyan balls. PbRCs from *Rhodobacter sphaeroides* and *Blastochloris viridis* have cytochrome c_2 and a bound tetraheme cytochrome as the source of electrons, respectively. In both PbRCs, the sources of electrons are at an equidistance of 20–21 Å from P_L and P_M. In PSII, W539 (21.4 Å), O4 (19.7 Å), and W1 (18.5 Å) are at similar distances (~20 Å) from the electron acceptor (monomeric $P_{D1}^{\bullet+}$).

D1] also (ii) facilitates release of protons from the substrate water molecules. These features seem to be the nature of PSII, which uses a protonated electron source—a pair of water molecules.

Methods

Coordinates and atomic partial charges

The atomic coordinates were taken from the X-ray structures; cyanobacterial PSI from *Thermosynechococcus elongatus* at 2.5 Å resolution (PDB code, 1JB0);[2] plant PSI from *Pisum sativum* at 2.8 Å resolution (PDB code, 4XK8); PbRC from *Rhodobacter sphaeroides* at 2.01 Å resolution (PDB code, 3I4D), 1.87 Å resolution (PDB code, 2J8C),[4] and 2.55 Å resolution (PDB code, 1M3X);[3] PbRC from *Thermochromatium tepidum* at 2.2 Å resolution (PDB code, 1EYS);[30] the PSII monomer unit (designated monomer A) of the PSII complexes from *Thermosynechococcus vulcanus* at 1.9 Å resolution (PDB code, 3ARC).[5] Hydrogen atoms were generated and energetically optimized with CHARMM.[54] Atomic partial charges of the amino acids were adopted from the all-atom CHARMM22) parameter set.[55] For PSI, the atomic charges of cofactors were taken from previous studies (Chl*a*, phylloquinone, β-carotene,[56] and the Fe_4S_4 cluster[57]). The atomic charges of the other cofactors ((B)Chl*a*, including (B) Chl$a^{\bullet+}$ and (B)Chl$a^{\bullet-}$, (B)Pheo*a*, ubiquinone, plastoquinone, spheroidene, sulfoquinovosyl diacylglycerol, heptyl 1-thiohexopyranoside, and the Fe complex) were determined by fitting the electrostatic potential in the neighborhood of these molecules using the RESP procedure[58] (Tables S2–S11†). To obtain the atomic charges of the Mn_4CaO_5 cluster or the Fe complex, backbone atoms are not included in the RESP procedure (except for D1-Ala344) (Table S11†). The electronic wave functions were calculated after geometry optimization by the DFT method with the B3LYP functional and 6-31G** basis sets, using the JAGUAR program.[59] For the atomic charges of the non-polar CH_n groups in cofactors (*e.g.*, the phytol chains of (B)Chl*a* and (B)Pheo*a* and the isoprene side-chains of quinones), the value of +0.09 was assigned for non-polar H atoms. We considered the Mn_4CaO_5 cluster to be fully deprotonated in S_1.

The protein inner spaces were represented implicitly with the dielectric constant $\varepsilon_w = 80$, whereas the following water molecules were represented explicitly; (i) for PSII, ligand water molecules of the Mn_4CaO_5 cluster (W1 to W4), a diamond-shaped cluster of water molecules near TyrZ (W5 to W7)[60], the water molecule distal to TyrD[44], ligand water molecules of Chl_{D1} (A1003 and D424), Chl_{D2} (A1009 and A359), and other Chl*a* (B1001, B1007, B1027, C816, and C1004); (ii) for PSI, clusters of water molecules near A_{1A} (A5007, A5015, A5022, A5043, and A5049) and A_{1B} (B5018, B5019, B5030, B5055, B5056, and B5058), ligand water molecules of A_{-1A} (B5005), A_{-1B} (A5005), and other Chl*a* (A5004, A5010, A5012, A5024, A5032, A5051, B5006, B5010, B5022, B5036, B5053, B5054, J127, L4023, and M155).

E_m calculation: solving the linear Poisson–Boltzmann equation

To obtain the E_m values in the proteins, we calculated the electrostatic energy difference between the two redox states in a reference model system by solving the linear Poisson–Boltzmann equation with the MEAD program[61] and using E_m(BChl*a*) = −641 mV, E_m(BPheo*a*) = −384 mV (based on E_m(BChl*a*) = −830 mV and E_m(BPheo*a*) = −600 mV for one-electron reduction measured in tetrahydrofuran,[62] considering the solvation energy difference), E_m(Chl*a*) = −798 mV, and E_m(Pheo*a*) = −641 mV (based on E_m(Chl*a*) = −910 mV and E_m(Pheo*a*) = −700 mV for one-electron reduction measured in butyronitrile[63]). The difference in the E_m value of the protein relative to the reference system was added to the known E_m value. The ensemble of the protonation patterns was sampled by the Monte Carlo method with Karlsberg.[64] The linear Poisson–Boltzmann equation was solved using a three-step grid-focusing procedure at resolutions of 2.5 Å, 1.0 Å, and 0.3 Å. Monte Carlo sampling yielded the probabilities $[A_{ox}]$ and $[A_{red}]$ of the two redox states of molecule A. E_m was evaluated using the Nernst equation. A bias potential was applied to obtain an equal amount of both redox states ($[A_{ox}] = [A_{red}]$), thereby yielding the redox midpoint potential as the resulting bias potential. To facilitate direct comparisons with previous computational results (*e.g.*,[13,26]), identical computational conditions and parameters were used; all computations were performed at 300 K, pH 7.0, and an ionic strength of 100 mM; the dielectric constants were set to $\varepsilon_p = 4$ inside the protein and $\varepsilon_w = 80$ for water.

Conflicts of interest

There are no conflicts to declare.

Acknowledgements

This research was supported by JST CREST (JPMJCR1656), JSPS KAKENHI (JP16H06560 and JP26105012), Japan Agency for Medical Research and Development (AMED), Materials Integration for engineering polymers of Cross-ministerial Strategic Innovation Promotion Program (SIP), and the Interdisciplinary Computational Science Program in CCS, University of Tsukuba.

References

1 H. Michel and J. Deisenhofer, *Biochemistry*, 1988, **27**, 1–7.
2 P. Jordan, P. Fromme, H. T. Witt, O. Klukas, W. Saenger and N. Krauss, *Nature*, 2001, **411**, 909–917.
3 A. Camara-Artigas, D. Brune and J. P. Allen, *Proc. Natl. Acad. Sci. U. S. A.*, 2002, **99**, 11055–11060.
4 J. Koepke, E. M. Krammer, A. R. Klingen, P. Sebban, G. M. Ullmann and G. Fritzsch, *J. Mol. Biol.*, 2007, **371**, 396–409.
5 Y. Umena, K. Kawakami, J.-R. Shen and N. Kamiya, *Nature*, 2011, **473**, 55–60.
6 X. Qin, M. Suga, T. Kuang and J. R. Shen, *Science*, 2015, **348**, 989–995.
7 T. Watanabe, M. Kobayashi, A. Hongu, M. Nakazato, T. Hiyama and N. Murata, *FEBS Lett.*, 1985, **191**, 252–256.
8 P. Joliot and A. Joliot, *Biochemistry*, 1999, **38**, 11130–11136.

9 T. Cardona, A. Sedoud, N. Cox and A. W. Rutherford, *Biochim. Biophys. Acta*, 2012, **1817**, 26–43.
10 J. C. Williams, R. G. Alden, H. A. Murchison, J. M. Peloquin, N. W. Woodbury and J. P. Allen, *Biochemistry*, 1992, **31**, 11029–11037.
11 V. V. Klimov, S. I. Allakhverdiev, S. Demeter and A. A. Krasnovskii, *Dokl. Akad. Nauk SSSR*, 1979, **249**, 227–230.
12 A. W. Rutherford, J. E. Mullet and A. R. Crofts, *FEBS Lett.*, 1981, **123**, 235–237.
13 K. Saito, T. Ishida, M. Sugiura, K. Kawakami, Y. Umena, N. Kamiya, J.-R. Shen and H. Ishikita, *J. Am. Chem. Soc.*, 2011, **133**, 14379–14388.
14 A. W. Rutherford, A. Boussac and P. Faller, *Biochim. Biophys. Acta*, 2004, **1655**, 222–230.
15 P. Faller, R. J. Debus, K. Brettel, M. Sugiura, A. W. Rutherford and A. Boussac, *Proc. Natl. Acad. Sci. U. S. A.*, 2001, **98**, 14368–14373.
16 H. Dau and M. Haumann, *Coord. Chem. Rev.*, 2008, **252**, 273–295.
17 M. Haumann and W. Junge, *Biochim. Biophys. Acta*, 1999, **1411**, 86–91.
18 J. S. Vrettos, J. Limburg and G. W. Brudvig, *Biochim. Biophys. Acta*, 2001, **1503**, 229–245.
19 G. Renger, *Biochim. Biophys. Acta*, 2001, **1503**, 210–228.
20 K. Saito, A. W. Rutherford and H. Ishikita, *Nat. Commun.*, 2015, **6**, 8488.
21 K. N. Ferreira, T. M. Iverson, K. Maghlaoui, J. Barber and S. Iwata, *Science*, 2004, **303**, 1831–1838.
22 H. Ishikita, W. Saenger, B. Loll, J. Biesiadka and E.-W. Knapp, *Biochemistry*, 2006, **45**, 2063–2071.
23 N. W. Woodbury and W. W. Parson, *Biochim. Biophys. Acta*, 1984, **767**, 345–361.
24 M. R. Gunner, A. Nicholls and B. Honig, *J. Phys. Chem.*, 1996, **100**, 4277–4291.
25 A. W. Rutherford, A. Osyczka and F. Rappaport, *FEBS Lett.*, 2012, **586**, 603–616.
26 H. Ishikita, W. Saenger, J. Biesiadka, B. Loll and E.-W. Knapp, *Proc. Natl. Acad. Sci. U. S. A.*, 2006, **103**, 9855–9860.
27 K. Saito and H. Ishikita, *Biophys. J.*, 2011, **101**, 2018–2025.
28 F. A. M. Kleinherenbrink, G. Hastings, B. P. Wittmershaus and R. E. Blankenship, *Biochemistry*, 1994, **33**, 3096–3105.
29 S. Kumazaki, M. Iwaki, I. Ikegami, H. Kandori, K. Yoshihara and S. Itoh, *J. Phys. Chem.*, 1994, **98**, 11220–11225.
30 T. Nogi, I. Fathir, M. Kobayashi, T. Nozawa and K. Miki, *Proc. Natl. Acad. Sci. U. S. A.*, 2000, **97**, 13561–13566.
31 H. Ishikita, J. Biesiadka, B. Loll, W. Saenger and E.-W. Knapp, *Angew. Chem., Int. Ed.*, 2006, **45**, 1964–1965.
32 B. Loll, J. Kern, W. Saenger, A. Zouni and J. Biesiadka, *Nature*, 2005, **438**, 1040–1044.
33 Y. Kato, M. Sugiura, A. Oda and T. Watanabe, *Proc. Natl. Acad. Sci. U. S. A.*, 2009, **106**, 17365–17370.
34 W. Holzapfel, U. Finkele, W. Kaiser, D. Oesterhelt, H. Scheer, H. U. Stilz and W. Zinth, *Chem. Phys. Lett.*, 1989, **160**, 1–7.
35 H. L. Axelrod, E. C. Abresch, M. Y. Okamura, A. P. Yeh, D. C. Rees and G. Feher, *J. Mol. Biol.*, 2002, **319**, 501–515.
36 M. Tetreault, S. H. Rongey, G. Feher and M. Y. Okamura, *Biochemistry*, 2001, **40**, 8452–8462.
37 W. W. Parson, Z.-T. Chu and A. Warshel, *Biochim. Biophys. Acta*, 1990, **1017**, 251–272.
38 U. Finkele, C. Lauterwasser, W. Zinth, K. A. Gray and D. Oesterhelt, *Biochemistry*, 1990, **29**, 8517–8521.
39 A. W. Roszak, K. McKendrick, A. T. Gardiner, I. A. Mitchell, N. W. Isaacs, R. J. Cogdell, H. Hashimoto and H. A. Frank, *Structure*, 2004, **12**, 765–773.
40 M. A. Steffen, K. Lao and S. G. Boxer, *Science*, 1994, **264**, 810–816.
41 N. Sakashita, H. C. Watanabe, T. Ikeda and H. Ishikita, *Photosynth. Res.*, 2017, **133**, 75–85.
42 N. Sakashita, H. C. Watanabe, T. Ikeda, K. Saito and H. Ishikita, *Biochemistry*, 2017, **56**, 3049–3057.
43 A. G. Gabdulkhakov, V. G. Kljashtorny and M. V. Dontsova, *Crystallogr. Rep.*, 2015, **60**, 884–888.
44 K. Saito, A. W. Rutherford and H. Ishikita, *Proc. Natl. Acad. Sci. U. S. A.*, 2013, **110**, 7690–7695.
45 R. J. Service, W. Hillier and R. J. Debus, *Biochemistry*, 2010, **49**, 6655–6669.
46 S. Nakamura and T. Noguchi, *Biochemistry*, 2015, **54**, 5045–5053.
47 K. Saito, N. Sakashita and H. Ishikita, *Aust. J. Chem.*, 2016, **69**, 991–998.
48 M. Zhang, M. Bommer, R. Chatterjee, R. Hussein, J. Yano, H. Dau, J. Kern, H. Dobbek and A. Zouni, *eLife*, 2017, **6**, e26933.
49 J. R. Durrant, D. R. Klug, S. L. Kwa, R. van Grondelle, G. Porter and J. P. Dekker, *Proc. Natl. Acad. Sci. U. S. A.*, 1995, **92**, 4798–4802.
50 G. Raszewski, B. A. Diner, E. Schlodder and T. Renger, *Biophys. J.*, 2008, **95**, 105–119.
51 N. W. Woodbury and J. P. Allen, in *Anoxygenic photosynthetic bacteria: advances in photosynthesis*, ed. R. E. Blankenship, M. T. Madigan and C. E. Bauer, Kluwer Academic Publishers, Dordrecht, 1995, pp. 527–557.
52 N. Cox, J. L. Hughes, R. Steffen, P. J. Smith, A. W. Rutherford, R. J. Pace and E. Krausz, *J. Phys. Chem. B*, 2009, **113**, 12364–12374.
53 B. A. Diner and F. Rappaport, *Annu. Rev. Plant Biol.*, 2002, **53**, 551–580.
54 B. R. Brooks, R. E. Bruccoleri, B. D. Olafson, D. J. States, S. Swaminathan and M. Karplus, *J. Comput. Chem.*, 1983, **4**, 187–217.
55 A. D. MacKerell Jr, D. Bashford, R. L. Bellott, R. L. Dunbrack Jr, J. D. Evanseck, M. J. Field, S. Fischer, J. Gao, H. Guo, S. Ha, D. Joseph-McCarthy, L. Kuchnir, K. Kuczera, F. T. K. Lau, C. Mattos, S. Michnick, T. Ngo, D. T. Nguyen, B. Prodhom, W. E. Reiher III, B. Roux, M. Schlenkrich, J. C. Smith, R. Stote, J. Straub, M. Watanabe, J. Wiorkiewicz-Kuczera, D. Yin and M. Karplus, *J. Phys. Chem. B*, 1998, **102**, 3586–3616.
56 K. Kawashima and H. Ishikita, *Biochemistry*, 2017, **56**, 3019–3028.
57 J. Mouesca, J. L. Chen, L. Noodleeman, D. Bashford and D. A. Case, *J. Am. Chem. Soc.*, 1994, **116**, 11898–11914.
58 C. I. Bayly, P. Cieplak, W. D. Cornell and P. A. Kollman, *J. Phys. Chem.*, 1993, **97**, 10269–10280.

59 *Jaguar*, version 7.9, Schrödinger, LLC, New York, NY, 2011.
60 K. Saito, J.-R. Shen, T. Ishida and H. Ishikita, *Biochemistry*, 2011, **50**, 9836–9844.
61 D. Bashford and M. Karplus, *Biochemistry*, 1990, **29**, 10219–10225.
62 T. M. Cotton and R. P. van Duyne, *J. Am. Chem. Soc.*, 1979, **101**, 7605–7612.
63 T. Watanabe and M. Kobayashi, in *Chlorophylls*, ed. H. Scheer, CRC Press, Boca Raton, FL, 1991, pp. 287–303.
64 B. Rabenstein and E. W. Knapp, *Biophys. J.*, 2001, **80**, 1141–1150.